Journal of Materials Processing Tech. 292 (2021) 117055

Contents lists available at ScienceDirect

Journal of Materials Processing Tech.

journal homepage: www.elsevier.com/locate/jmatprotec

Electrochemical polishing of microfluidic moulds made of tungsten using a bi-layer electrolyte

Xingying Zhou [a], Fang Wang [a,b], Xinquan Zhang [c,*], Hui Deng [a,*]

[a] Department of Mechanical and Energy Engineering, Southern University of Science and Technology, No. 1088, Xueyuan Road, Shenzhen, Guangdong, 518055, China
[b] Department of Mechanical Engineering, University of Hong Kong, 999077, Hong Kong
[c] School of Mechanical Engineering, Shanghai Jiao Tong University, Shanghai, 200240, China

ARTICLE INFO

Associate Editor: Dr Jian Cao

Keywords:
Microfluidic mould
Tungsten mould
Electrochemical polishing
Bi-layer electrolyte
Surface roughness

ABSTRACT

Microfluidic chips made of glass are important analytical devices for applications in biomedicine, drug development and chemical analysis. For the mass production of glass-based microfluidic chips, tungsten-made microfluidic moulds are indispensable. In this paper, a dynamic electrochemical polishing (ECP) process using a bi-layer NaOH electrolyte is proposed to uniformly polish tungsten moulds. The ECP conditions are optimized to determine the best anode potential and polishing duration. The problem of pitting during ECP can be solved by an ultra-short ECP post-treatment of several seconds. During static ECP, the material removal on the mould is nonuniform, and material removal uniformity is greatly improved by dynamic ECP. After 10 cycles of dynamic ECP, a tungsten mould with a mirror surface is obtained, and the surface roughness (Sa) is drastically reduced from 205.98 nm to 4.14 nm. The results presented in this paper demonstrate that dynamic ECP is a promising approach for highly efficient and uniform polishing of tungsten moulds with microscopic features.

1. Introduction

Currently, an increasing number of microfluidic devices are being developed and applied in various fields, such as biomedicine, pharmacy and chemical analysis (Lee, 2014). For instance, Madou et al. (2001) developed a polymer-based microfluidic platform that can integrate various microfluidic functions, such as flow sequencing, cascade micro mixing and capillary metering. Takagi et al. (2005) proposed a new method for continuous particle size separation and particle collection using laminar flow in microchannels. Moreover, Andersson and Van (2004) showed that cell patterning and topographical control over cells can be realized on the basis of microfluidic systems.

Microfluidic chips are generally made from thermoplastics, such as polydimethyl siloxane (PDMS), polycarbonate (PC) and polymethyl methacrylate (PMMA), because these materials can be fabricated easily at a low cost (Tan et al., 2001). Moreover, the surfaces of thermoplastics can be easily modified through many chemical methods (Dominick et al., 2003). However, the heat resistance and chemical resistance of these materials are weak, which makes them difficult to work in high temperature and organic environments (Huang et al., 2012). Glass, which has good resistance to chemical corrosion and thermal deformation, is a promising material for microfluidic chips (Chen et al., 2006). Traditional glass-based microfluidic chips are mainly produced by wet etching processes using a hydrofluoric acid solution, which is expensive and dangerous (Zhang et al., 2015). Compared with wet etching, glass moulding is an efficient approach for mass production of glass components (Zhou et al., 2011). In this paper, tungsten is selected as the mould material for the moulding of glass-based microfluidic devices. Tungsten has a sufficient hardness and better machinability compared with that of SiC and WC (Suzuki et al., 2007). For the fabrication of tungsten moulds, the required microscopic features are generally machined by micro milling (Altan et al., 1993), and then polishing is carried out to improve the surface quality (Guo et al., 2012). Magnetorheological polishing (MRF) (Wang et al., 2015) and chemical mechanical polishing (CMP) (Saka et al., 2008) are common methods for polishing optical moulds. However, MRF and CMP are both tool-based removal processes that are not applicable for polishing surfaces with microscopic features. Thus, in this report, electrochemical polishing (ECP), which is based on electrochemical etching and is a noncontact polishing process, is utilized to polish tungsten microfluidic moulds with good surface roughness and dimensional accuracy.

In previous studies, it has been suggested that ultra-smooth tungsten surfaces with a subnanometer roughness can be successfully obtained by ECP (Prihandana et al., 2013). During the ECP process, a viscous layer

* Corresponding authors.
E-mail addresses: zhangxinquan@sjtu.edu.cn (X. Zhang), dengh@sustech.edu.cn (H. Deng).

https://doi.org/10.1016/j.jmatprotec.2021.117055
Received 3 August 2020; Received in revised form 6 December 2020; Accepted 11 January 2021
Available online 19 January 2021
0924-0136/© 2021 Published by Elsevier B.V.

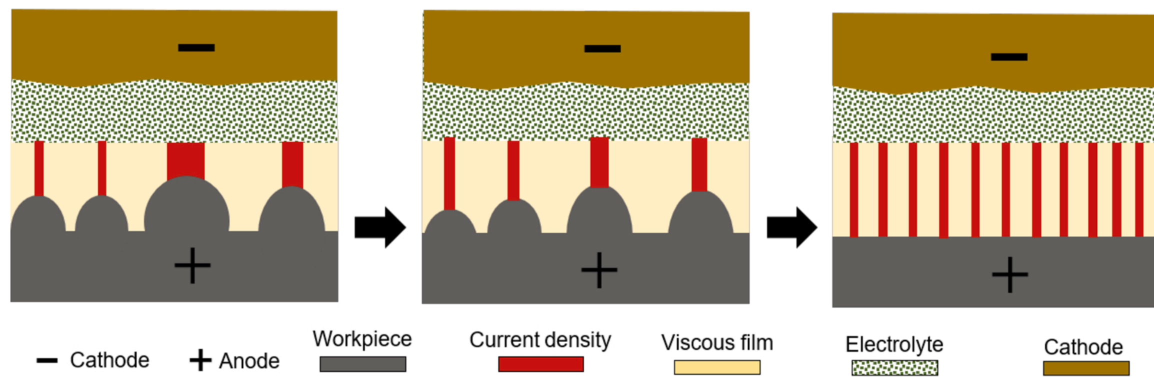

Fig. 1. Schematic of the ECP mechanism based on "viscous film theory".

with high electric resistance is formed on a metal surface. The polishing effect of ECP is based on the different etching rates at peak and valley sites owing to the different thicknesses of the viscous layer (Han and Fang, 2019). In the traditional ECP method, the sample to be polished is completely immersed in the electrolyte during polishing. Thus, the whole surfaces of small parts can be effectively polished (Wang et al., 2019). However, when ECP is used to polish large samples with microscopic structures, the variation in the viscous layer thickness and electric field distribution results in a nonuniformity in the material removal in different regions on the mould, which causes dimensional error. When there are patterns on the mould surface, the thickness of the viscous layer at the top and bottom region is different owing to the flowing of the viscous layer under the influence of the gravity. Moreover, the ion diffusion rate between the mould and the cathode, which is governed by the electric field, is closely related to the geometry of the apparatus and the dimension of the mould and electrode (Elmore, 1939). Thus, for polishing of large components by ECP, dimensional and form errors are inevitably introduced (Hopenfeld and Cole, 1966).

To solve the problem of the nonuniformity of material removal in the traditional immersion-based ECP method (static ECP), a dynamic ECP method using a bi-layer electrolyte that can achieve uniform polishing of moulds with large dimensions is proposed in this work. Unlike the static ECP process in which the mould is completely immersed in electrolyte, the proposed dynamic ECP process only uses a very thin floating layer of solution as the electrolyte. As electrochemical etching is restricted to a thin electrolyte layer and the mould passes through the floating electrolyte at a constant speed, the variation in material removal on the mould surface is reduced, and finally, the mould can be polished with good uniformity. In this study, static and dynamic ECP processes were comparatively studied. The polishing characteristics of static ECP with an immersion mode and dynamic ECP using a bi-layer electrolyte are presented.

2. Principles of ECP and experimental apparatus

ECP is a finishing process that removes material from a metal sample based on an anode dissolution process (Han and Fang, 2019). Although the ECP process has a relatively long history, the specific polishing mechanism is not yet fully understood. The most widely accepted polishing mechanism is the "viscous film theory" first proposed by Jacquet (1936).

Fig. 1 shows a schematic diagram of the ECP mechanism based on "viscous film theory". During the ECP process, a very thin viscous film forms on the surface of the anode (metal substrate). This film has a greater electric resistance and viscosity than those of the bulk electrolyte solution. The thickness of the viscous film is not even due to the rough morphology of the anode surface. Thus, the thickness of the viscous film is relatively low on large protrusions, so the corresponding resistance is low and the current density is high, which results in a large dissolution

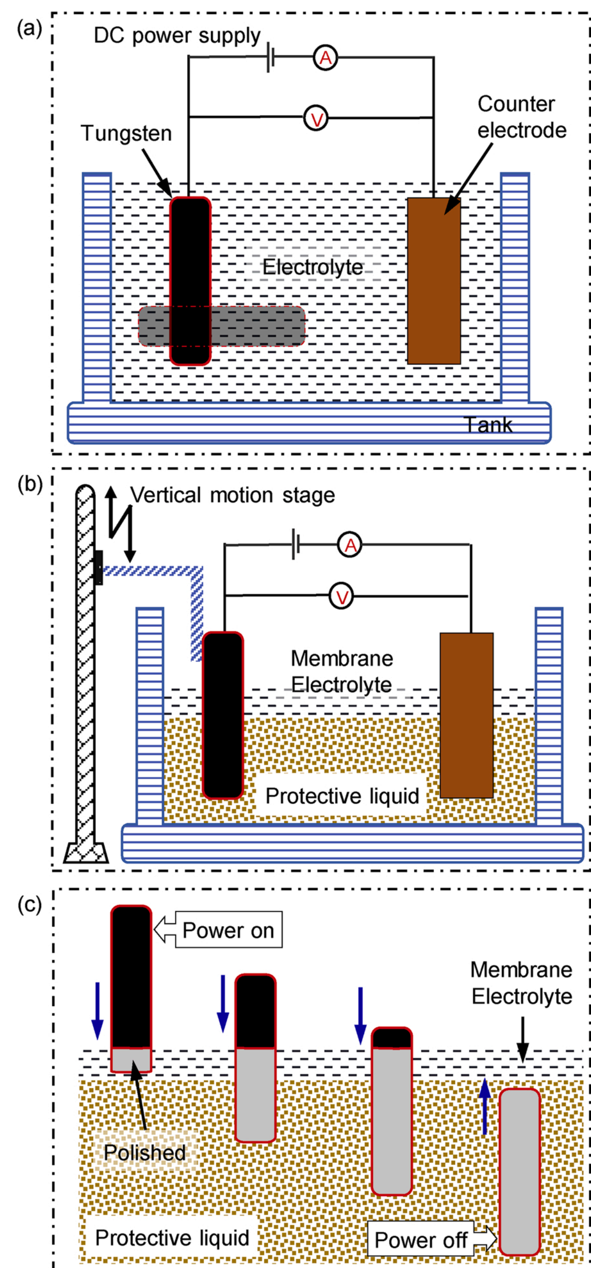

Fig. 2. Schematics of the experimental apparatuses. (a) The traditional immersion-based ECP setup; (b) the proposed dynamic ECP setup based on bi-layer electrolyte; and (c) one polishing cycle of the mould during dynamic ECP.

rate. In contrast, the viscous film is relatively thick at the small protrusion sites, and the material dissolution rate is low due to the low current density. As the reaction progresses, the different current densities on the small and large protrusion sites lead to different etching rates, and the anode surface is eventually smoothed.

A schematic of the experimental apparatus used for traditional immersion-based ECP is shown in Fig. 2(a). The workpiece is completely immersed into the electrolyte. In this polishing method, when the workpiece is placed vertically, the viscous film on the surface flows downward due to gravity. Therefore, the viscous film on the upper and lower regions has different thicknesses, which results in different etching rates and polishing effects. If the workpiece is placed horizontally, the electric field difference between the two ends of the workpiece is large; thus, the etching rate and polishing effect on different regions on the mould are also different. In other words, the immersion-based static ECP method has poor polishing uniformity.

The abovementioned problem is considered to be solved by the proposed dynamic ECP approach. Fig. 2(b) shows a schematic of the dynamic ECP experimental apparatus based on a bi-layer electrolyte. A beaker with a volume of 900 mL is used as the electrolytic cell. Fluorocarbon ether is used to protect the polished area of the sample from further reactions. NaOH solution with a concentration of 0.5 wt% is used as the electrolyte. Owing to the poor intermiscibility and large density difference, NaOH solution is floating on fluorocarbon ether to realize the ECP with bi-layer electrolyte. The thickness of the NaOH layer can be controlled by adjusting its volume. In this study, the thickness was 10 mm to balance the polishing uniformity and efficiency. The tungsten mould connected to the positive terminal of a DC power supply served as the anode, and a platinum sheet (30 mm × 30 mm) served as the counter electrode.

As shown in Fig. 2(c), the mould was mounted on a numerically controlled vertical axis. Before the experiment, the displacement and moving speed of the workpiece is input into the computer control software interface. According to the relationship between the displacement and the speed, the time that power supply needs to be powered on in a polishing cycle is obtained. During the dynamic ECP process, the mould was moving down at a constant speed to achieve polishing of the entire surface. During the moving process, the surface region in contact with the NaOH electrolyte was selectively polished, while the surface immersed in fluorocarbon ether was protected. When the sample completely passed through the electrolyte, the power is automatically turned off and one cycle of dynamic ECP finished. Further polishing of the mould with more cycles is also possible by programming. The distance between the substrate and the counter electrode was 70 mm. Before polishing, ultrasonic cleaning with alcohol was carried out to remove particles and organic contaminations on the surface of the mould. After polishing, the mould was rinsed in deionized water and dried by blowing N_2. Since the samples were fully rinsed and dried before and after each experiment, it can be considered that they are free of contamination during multiple characterization analyses and multiple experiments.

EP of tungsten alloy can be considered as a reaction process in which anodic oxidation and dissolution occur simultaneously. The anodized product WO_3 from tungsten alloy can be quickly dissolved in NaOH solution, which used as the electrolyte in this study. The electrochemical reactions occurring on the platinum sheet (cathode) and tungsten (anode) can be expressed as follows:

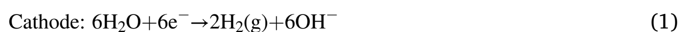

$$\text{Cathode: } 6H_2O+6e^- \rightarrow 2H_2(g)+6OH^- \quad (1)$$

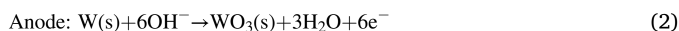

$$\text{Anode: } W(s)+6OH^- \rightarrow WO_3(s)+3H_2O+6e^- \quad (2)$$

$$WO_3(s)+2OH^- \rightarrow WO_4^{2-}+H_2O \quad (3)$$

During the EP process, the anodic oxidation reaction of tungsten alloy follows Eq. (2), and the tungsten oxide WO_3 dissolution reaction follows Eq. (3). The hydrogen evolution reaction that occurs at the cathode follows Eq. (1).

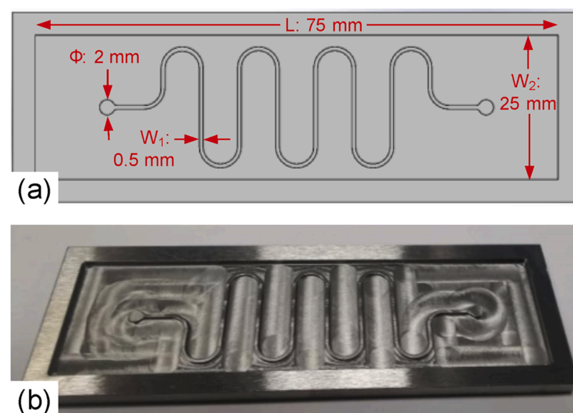

Fig. 3. CAD drawing (a) and photo (b) of the tungsten microfluidic mould.

The surface morphology of the tungsten mould before and after ECP was observed by scanning electron microscopy (SEM, Hitachi S-4800). Surface roughnesses with different scales were evaluated by atomic force microscope (AFM, BRUKER Dimension edge) and a scanning white light interferometer (SWLI, Taylor Hobson M112-4449-02 CCI HD). The dimensions of the features on the mould were measured by surface profilometer (SURFCOM NEX 031 DX-12).

3. Microfluidic mould made of tungsten

In this study, a raw mould made of a tungsten alloy with a purity of 99.99 % (supplied by Plansee Corp.) was first milled to fabricate the fluidic microfeatures. Fig. 3 shows the CAD drawing of the mould and a photograph of the milled mould. The central area of the mould is the characteristic structure used to fabricate the microchannel on glass products.

Before the polishing experiment, SEM was used to observe the surface morphology of the mould. As the surface was obtained by milling, obvious milling marks can be observed on the low-magnification SEM images shown in Fig. 4(a–c), and the surface appears very rough. When the surface was observed with high magnification as shown in Fig. 4 (d–f), various surface defects introduced by milling can be seen clearly, such as a wavy indentation morphology caused by uneven surface extrusion, burning caused overheating and migration and adhesion caused by mechanical plowing.

4. Static ECP with an immersion mode

According to the classic anode current density-potential curve, the anode potential plays an important role in the static ECP process. Therefore, in this study, the effect of the anode potential on the surface roughness and surface morphology of the substrate was studied first. Nine tungsten samples were processed by ECP with different anode potentials in the range from 2 to 60 V, and the duration of each polishing process was 5 min. After ECP, the surface roughness was evaluated using SWLI, and the surface morphology was observed using SEM.

Over the entire potential range from 2 to 60 V, the dependence of the surface roughness on the applied potential is shown in Fig. 5. It was found that the surface roughness first increased with an increase in the anode potential and reached the maximum value (Sa of 116.32 nm) at 5 V. As reported, the roughness of the sample surface increased at low anode potentials due to the etching on the surface, which is also called the etching stage of ECP. When the anode potential was increased from 5 to 10 V, the surface roughness quickly decreased from a Sa of 116.32 nm to 72.16 nm. This is because the potential range from 5 to 10 V is considered a transition range from the etching stage to the smoothening stage, so a slight increase in the anode potential causes a significant

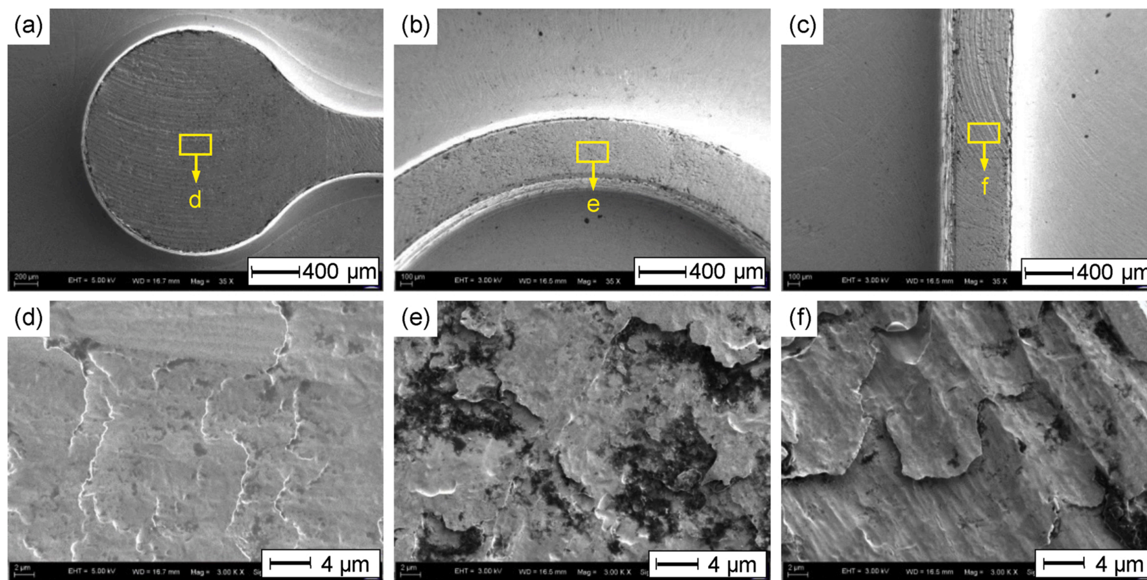

Fig. 4. Morphology of the milled tungsten mould before ECP observed by SEM. (a–c) Three typical feature sites on the mould (35X). (d–f) Detailed surface morphology of the feature sites (3000×).

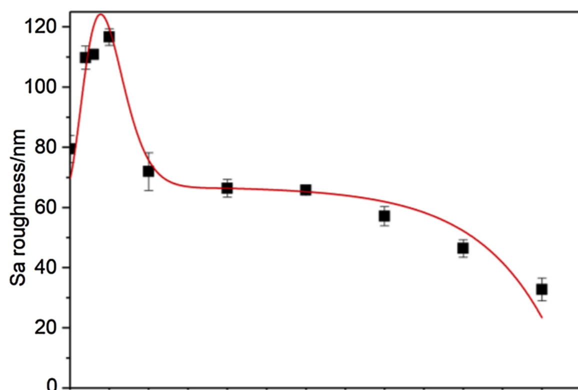

Fig. 5. Dependency of surface roughness Sa under the anode potential.

reduction in the surface roughness. When the anode potential was in the range from 10 to 60 V, the Sa gradually decreased as the potential increased. When the anode potential was increased to 60 V, the surface roughness dropped to Sa 33.41 nm. It is noteworthy that the Sa can be further reduced by prolonging ECP duration with an anode potential of 60 V. The curve shown in Fig. 5 demonstrates that 5–10 V is the transition potential range between roughening and smoothening, and a higher potential is desired to realize highly efficient ECP of tungsten.

Fig. 6 shows the surface morphology of the as-received tungsten substrate and after ECP at 5 V and 60 V for 5 min. Fig. 5 reveals that 5 V is in the roughening range of ECP; thus, the surface processed by ECP under 5 V is still rough, although defects such as cracks and scratches on the original surface were completely removed. As shown in Fig. 6(e), grain boundaries can be observed, demonstrating that 5 V of anode potential caused an orientation-dependent etching process during ECP. When the applied anode potential was 60 V, a smooth surface was obtained. As shown in images (c) and (f), the defects on the original surface

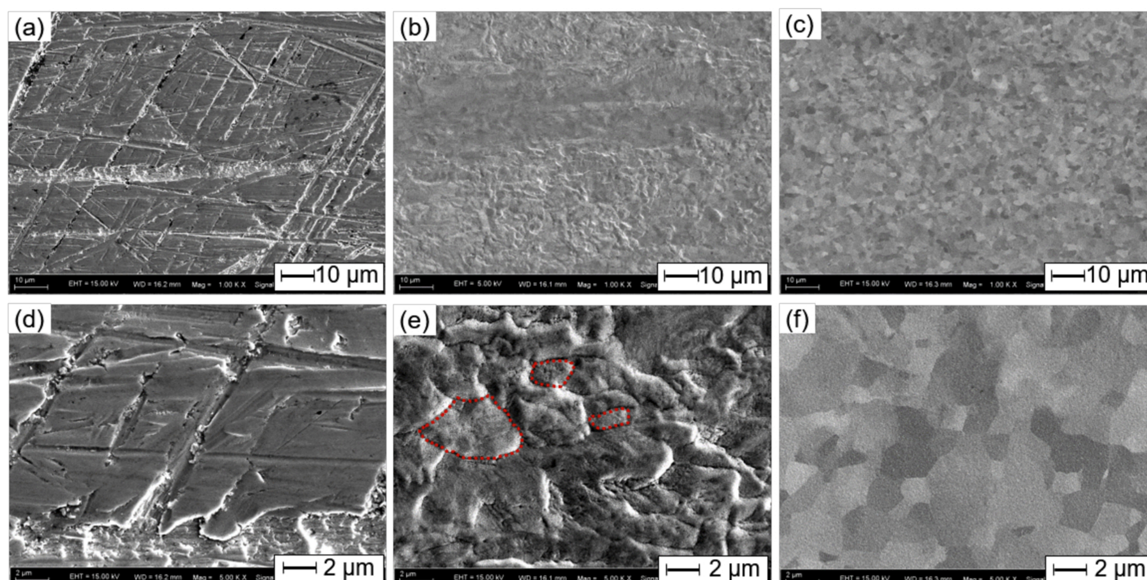

Fig. 6. SEM images of the as-received and ECP-processed tungsten substrate. (a, d) Original surface. (b, e) 5 V and 5 min. (c, f) 60 V and 5 min.

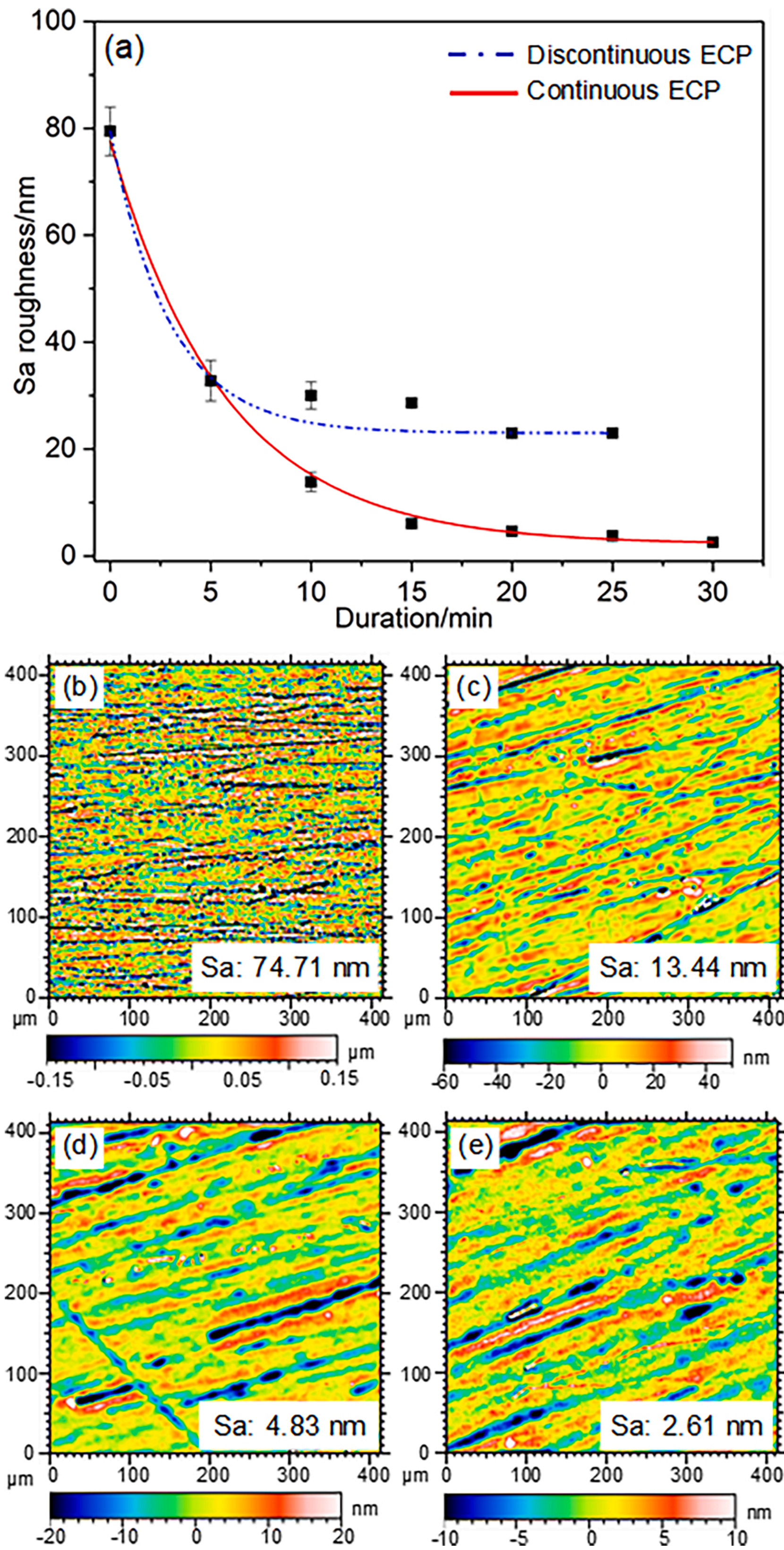

Fig. 7. (a) Roughness variation during ECP with multiple cycles and continuous ECP. (b) SWLI of original surface. (c-e) SWLI images of the tungsten surface processed by continuous ECP with different durations; (c) ECP for 10 min; (d) ECP for 20 min; and (e) ECP for 30 min.

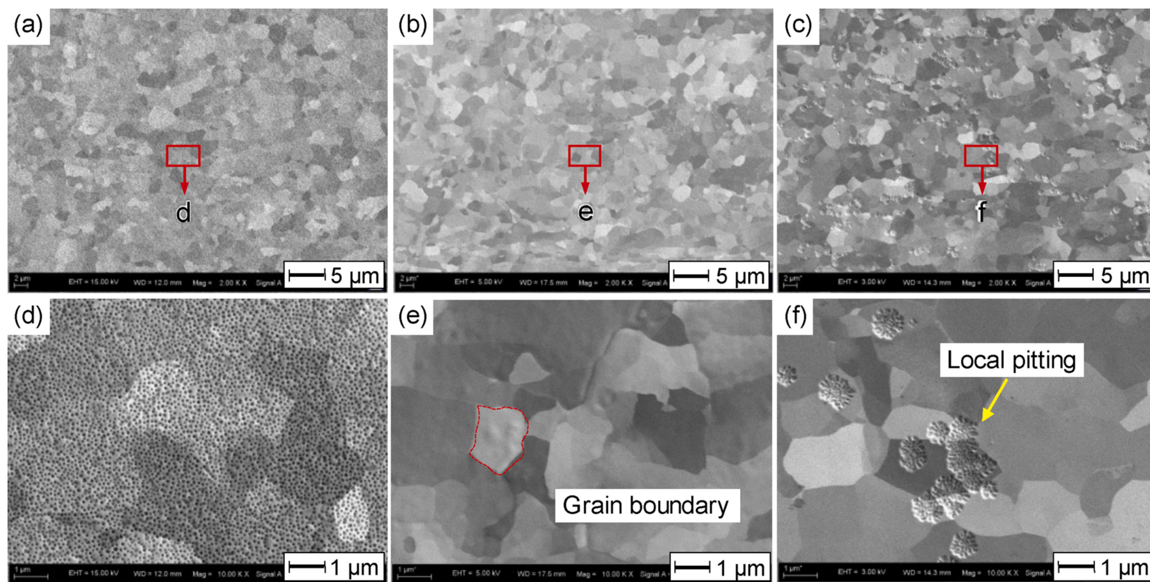

Fig. 8. Three different surface morphologies were obtained after ECP at 60 V. (a and d): continuous ECP for 30 min; (b and e): further processed by ECP for 5 s; (c and f): further processed by ECP for 30 s.

were removed completely without the introduction of rough etching marks, and an ultra-smooth surface with clear grain structure was obtained.

Compared with (f) in the Fig. 6, the grain boundary of (e) is not obvious. The main reason is that the initial sample surface used in the etching experiment was a surface obtained by mechanical grinding. This surface was full of surface defects caused by mechanical processing, and the orientation difference between the crystal grains became blurred. Therefore, when a low-potential ECP is applied to it, the crystal grain boundary becomes difficult to identify. Although the grain boundary in image (e) is not obvious, there are still several clear closed-loop boundaries. As the size of these red boxes is close to the grain size in image (f), it is considered that the red boxes could represent the grain boundary after etching.

The above experiments show that the anode potential has an important influence on the surface morphology of the tungsten processed by ECP. A high anode potential is preferred to improve the surface roughness. Thus, in the following experiments for static and dynamic ECP, 60 V was selected as the anode potential.

The surface roughness variation under different cumulative polishing durations was investigated. ECP with multiple cycles and continuous ECP were conducted, and Fig. 7 shows the results. A tungsten sample was processed with 5 cycles of static ECP with one cycle duration of 5 min. After each polishing cycle, the surface roughness was measured by SWLI. The blue curve illustrated in Fig. 7(a) shows the roughness variation of the tungsten during ECP with multiple cycles. The roughness decreased drastically after the first polishing cycle of 5 min. However, the roughness did not change significantly even if more ECP cycles were conducted. After 5 cycles of polishing, the surface roughness of the sample was finally decreased to a Sa of 22.30 nm. However, this roughness value still did not meet the high-quality surface requirements of the glass mould. The unsatisfactory polishing after an ECP processes with multiple cycles was probably due to the insufficient formation of a viscous layer. According to the mechanism of ECP, if the thickness of the viscous layer is too small, and is comparable to the peak-to-valley distance on the surface, a smoothening effect originating from different etching rates at the peaks and valleys cannot be realized.

Continuous ECP with different polishing durations was carried out using six different tungsten samples as the polishing duration increased from 5 to 30 min. The relationship between the surface roughness and polishing duration is shown in the red curve in Fig. 7(a). After 10 min of continuous ECP, the surface roughness was reduced to a Sa of 13.44 nm. When the polishing time exceeded 20 min, the polished surface became ultra-smooth, and the best Sa of 2.61 nm was achieved after polishing for 30 min, as shown in Fig. 7(e). The detailed surface morphology variation during continuous ECP is shown in Fig. 7(b–e). It is obvious that the number of scratches on the surface was significantly reduced after 10 min of polishing. With an increase in the ECP duration, shallow scratches disappeared, and the deep scratches expanded. Based on the results shown in Fig. 7, it can be concluded that during static ECP, a long polishing duration is indeed helpful to achieve a smooth surface with a low roughness.

The better performance in continuous polishing may be caused by the increasing temperature of electrolyte during the polishing process. As the temperature increases, the effect of ECP becomes more active due to the low viscosity and continuous supply of fresh electrolyte. This process strengthens the selective dissolution between the prominent position and valley position (Caire et al., 1993). In addition, the current density increases with increasing temperature, and a higher current density contributes to better ECP effect due to the better surface roughness (Han and Fang, 2019).

Though an ultra-smooth surface can be obtained by ECP with a high anode potential, the polished surface was fully covered by nano pits. As the pits were too small, the surface roughness did not deteriorate when measuring with SWLI. However, as the surface hardness was affected by the nano pits, which further affected its performance during moulding, a post treatment approach was evaluated to solve the pitting problem. During static ECP, it has been discovered that there are three main types of morphologies on the surface of tungsten processed by ECP with a high anode potential of 60 V. They can be described as completely pitted surfaces, locally pitted surfaces and completely pit-free surfaces. As shown in Fig. 8(a) and (d), when one sample was processed by ECP for 30 min, the surface became completely covered with nano pits. However, if a short polishing time of 5 s was further applied to this sample, the dense covered pits disappeared, and a completely pit-free surface with clear grain boundaries was obtained, as shown in Fig. 8(b) and (e). If the sample was further processed by ECP for 30 s, locally pitted sites were observed, as shown in Fig. 8(c) and (f). Moreover, it was revealed that the formation of pits had no selectivity for grain boundaries or grain orientations and that they were randomly formed on the surface. In summary, when the surface after high-potential polishing was full of nano pits, an ultra-short ECP post-treatment can be performed on this

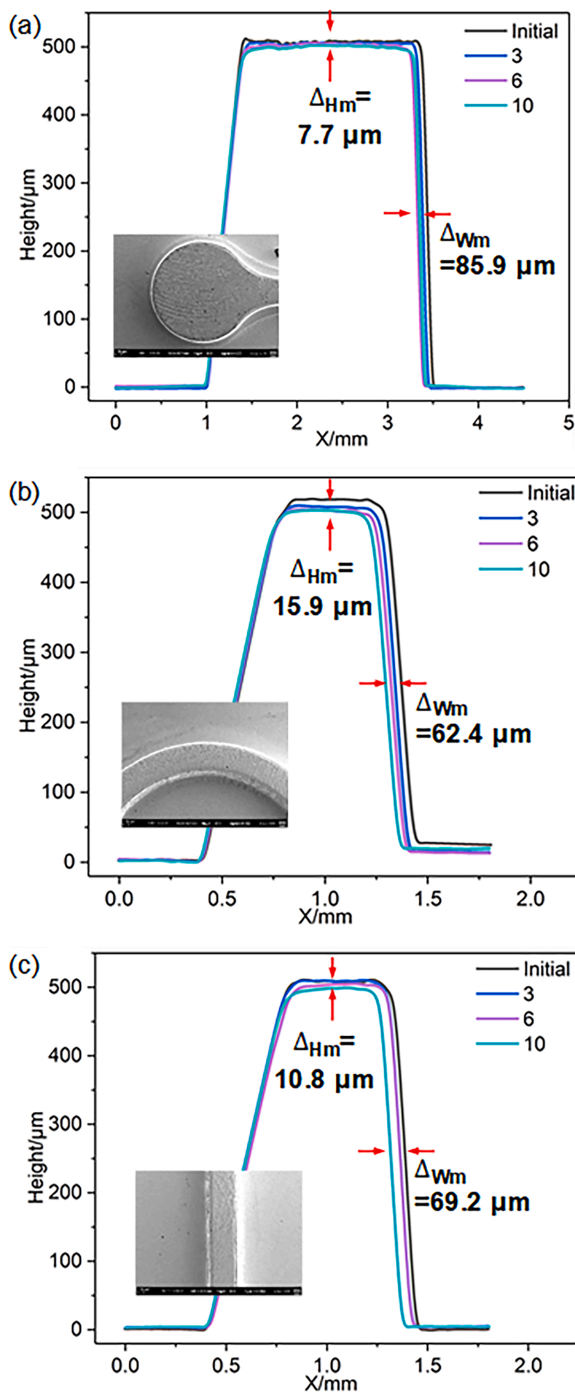

Fig. 9. Dimensional changes during immersion-based ECP at 3 typical feature sites in the mould. (a) Circular boss structure. (b) Curved boss structure. (c) Straight boss structure.

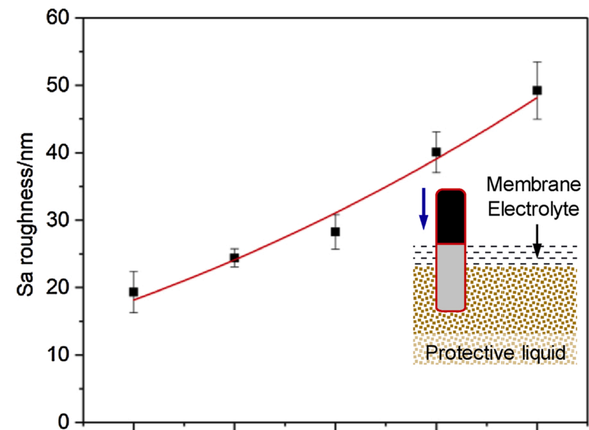

Fig. 10. Relationship between surface Sa roughness and sinking speed of the mould.

sample to eliminate the pits. The so-called ultra-short time ECP post-treatment is to clean and dry the sample and then perform an ECP with a very short polishing time, such as 5 s. Although there is no difference between the processed sample and the pre-processed sample under observation with the naked eye, the nano pits do disappear under the SEM.

During ECP, the probable mechanism for the formation of nano pits varies with the type of metal material and electrolyte. The formation of small pits on the surface of iron and nickel in a chlorine-containing electrolyte is considered to be caused by chloride ions attacking the passive film on the anode surface during polishing (Strehblow and Ives, 1976). The formation of hemispherical pits on the surface of titanium in a bromine-containing electrolyte is considered to be caused by the excessive current density at the potential pit cores on the metal surface (Beck and Alkire, 1979). In this study, for the ECP of tungsten using NaOH, the pitting mechanism is still not clear and needs to be further studied. However, the results shown in Fig. 8 prove that post treatment by ECP with an ultra-short duration of several seconds is a promising approach to remove nano pits.

The material removal uniformity of immersion-based ECP was investigated. The mould was vertically mounted using the apparatus shown in Fig. 2(a). The dimensional change of the features on the mould was evaluated using the profilometer. For an improved comparison with the bi-layer dynamic ECP process, immersion–based ECP was performed with multiple cycles. In this experiment, each polishing cycle was chosen to be 250 s ensure that the polishing time per unit area of the mould was the same for as that for static ECP.

The cross-sectional profiles of the three typical feature sites before and after static ECP with 3, 6, and 10 cycles were measured, as shown in Fig. 9. After 10 cycles of ECP, the height changes of these three feature sites were 7.7, 15.9 and 10.8 μm. The maximum difference in the height variation in the different locations was 8.2 μm. On the other hand, the width reduction of these three features was 85.9, 62.4, and 69.2 μm. The maximum difference in the width variation in the different locations was 23.5 μm. The results shown in Fig. 9 demonstrate that the material

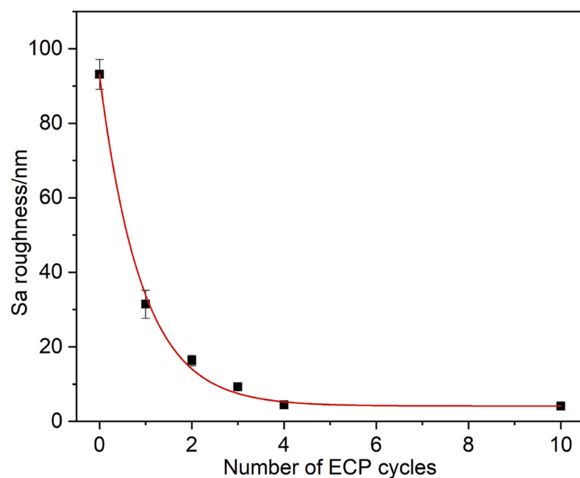

Fig. 11. Relationship between surface Sa roughness and number of dynamic ECP cycles.

removal rate in different areas of the mould was nonuniform during the immersion-based static ECP process.

5. Dynamic ECP using a bi-layer electrolyte

To solve the problem of uneven material removal caused by an excessive surface potential difference and the different thicknesses of the viscous layer during static ECP, a dynamic ECP process using bi-layer electrolyte was evaluated. To achieve polishing of the whole mould surface, the mould needs to move down at a constant speed during the polishing process. Since the movement of the workpiece during ECP may affect the state of the viscous film, the effect of the sample moving speed on the surface roughness was studied. Dynamic ECP with different moving speeds from 40 to 60 μm/s was conducted on five different samples, and the Sa roughness of these samples after one cycle of polishing was measured with SWLI.

As shown in Fig. 10, the roughness value of the polished sample increased when the sample sunk at an increased speed. There are two reasons to explain this result. First, when the moving speed of the sample increased, the polishing time per unit area decreased, so the surface roughness cannot be effectively reduced. Second, with a fast sinking speed, it was difficult to form a stable viscous layer; thus, the polishing effect was weakened. On the other hand, the moving speed of the mould in dynamic ECP cannot be too low. A low moving speed could cause a large amount of heat to accumulate in the anode surface and in the electrolyte during polishing. When a moving speed below 40 μm/s was tried, the protective liquid, which has a low boiling point, boiled and hindered the polishing process. Therefore, for the dynamic ECP of the tungsten mould, 40 μm/s was selected as the moving speed.

It is obvious that the surface produced by one cycle of dynamic ECP with a moving speed of 40 μm/s was not smooth enough for the moulding of glass. Thus, dynamic ECP with multiple cycles was carried out on one sample. As shown in Fig. 11, after four cycles of dynamic ECP, the surface roughness of the mould decreased from a Sa of 93.16 nm to 4.45 nm, which is comparable to that of the conventional static ECP process. Moreover, with a further increase in the number of ECP cycles, the decrease in the Sa roughness was not significant.

Under the optimized conditions (thickness of NaOH electrolyte: 10 mm, anode potential: 60 V, and moving speed: 40 μm/s), dynamic ECP of a raw mould was carried out, as shown in Fig. 3. To effectively eliminate surface defects and create a smooth surface, dynamic ECP was performed 10 times. After the ECP process, SEM observation of the feature sites with different magnifications was conducted and compared with those of the raw mould, as shown in Fig. 4.

Fig. 12 shows the morphologies of three typical feature sites on the polished mould. The surface of these three feature sites became smooth after ECP, and the milling marks as well as other defects shown in Fig. 4 were effectively removed. From the high-magnification images, it can be seen that the grain boundaries were clear at all sites, demonstrating that dynamic ECP has the capability to smooth the whole tungsten mould by passing through the floating electrolyte, although the polishing uniformity needs to be further investigated.

The dimensional changes caused by dynamic ECP were evaluated using a profilometer. Fig. 13 shows the cross-section profiles of the three typical feature sites processed by dynamic ECP with different numbers of cycles. After 10 dynamic ECP cycles, the height changes of these three feature sites were 4.3 μm, 4.9 μm and 4.9 μm. The maximum difference in the height variation in different locations was 0.6 μm, which is much smaller than that caused by the immersion-based static ECP process. On the other hand, after 10 dynamic ECP cycles, the width reduction of these three feature sites was relatively large and was 81.5 μm, 75.3 μm,

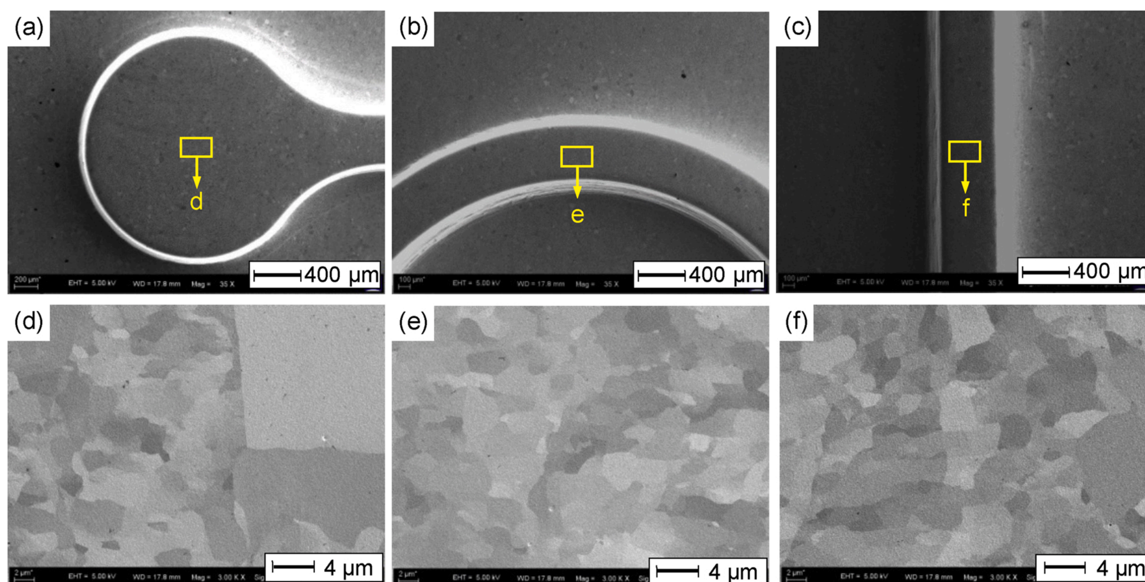

Fig. 12. Morphologies of the milled tungsten mould after ECP observed by SEM. (a–c) Three typical feature sites on the mould (35X). (d–f) Detailed surface morphology of the feature sites (3000×).

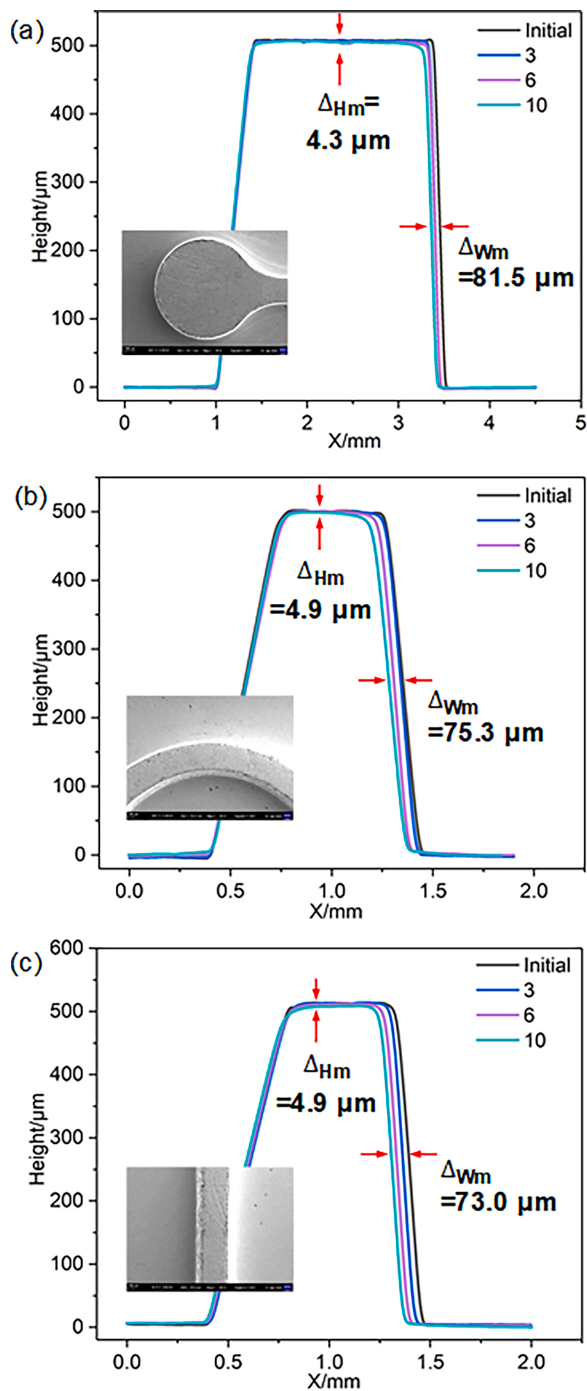

Fig. 13. Dimensional changes caused by bi-layer dynamic ECP at 3 typical feature sites in the mould. (a) Circular boss structure. (b) Curved boss structure. (c) Straight boss structure.

and 73.0 μm. The maximum difference in the width variation at different locations was 8.5 μm, which is also much smaller than that caused by static ECP. Compared with the results shown in Fig. 9, it can be concluded that the uniformity of material removal was greatly improved by the proposed dynamic ECP process in terms of both in the height and width dimensions.

Fig. 14 shows a comparison of the raw mould and polished mould processed by the dynamic ECP process. The surface of the mould after dynamic ECP is bright and has a significant mirror-like finish. The roughness change before and after polishing was evaluated using SWLI and AFM with different measuring scales. On the raw mould, milling marks can be observed, as shown in Fig. 14(b). Fig. 14(e) shows the SWLI image of the polished surface. The milling marks were completely removed, and the surface roughness was reduced from a Sa of 205.98 nm to 4.14 nm. In addition, AFM was used to evaluate the roughness and morphology on a microscopic scale. As shown in Fig. 14(c), there were many burrs and warping from debris on the surface due to the action of the mechanical plow. In contrast, these defects disappeared on the polished surface, as shown in Fig. 14(f). It is noteworthy that the polished mould surface was free of subsurface damage, as ECP is an etching-based material removal process.

6. Conclusions

In this study, a dynamic ECP process using a bi-layer electrolyte was proposed for the uniform polishing of tungsten-made microfluidic mould with micro features. The ECP conditions were optimized. A comparative study between immersion-based static ECP and dynamic ECP was conducted. It was indicated that dynamic ECP is a promising approach for polishing tungsten moulds with an excellent surface quality and polishing uniformity. To summarize, the following conclusions can be drawn from this study:

- The anode potential has an important influence on the polishing effect of ECP. For the developed ECP apparatus, 5 V is the critical potential for the transition from roughening to smoothing. A higher anode potential is preferred to achieve better surface roughness.
- An ultra-smooth tungsten surface with the best Sa roughness of 2.61 nm can be achieved by ECP for 30 min. The pitting phenomenon in ECP has been studied. Nano pits can be effectively removed by an ultra-short ECP post-treatment of several seconds.
- In static ECP, material removal on the mould is nonuniform owing to the nonuniform distribution of the viscous layer and the electric field. Thus, the dimensional changes of the mould features are greatly different. The difference in height variation is 8.2 μm, and the difference in width variation is 23.5 μm.
- During dynamic ECP, an improved polishing effect can be obtained when the movement speed of the sample is 40 μm/s. After 10 cycles of dynamic ECP, the surface roughness can be decreased from a Sa of 205.98 nm to 4.14 nm. Moreover, the difference in the height variation is decreased to 0.6 μm, and the difference in width variation is decreased to 8.5 μm.

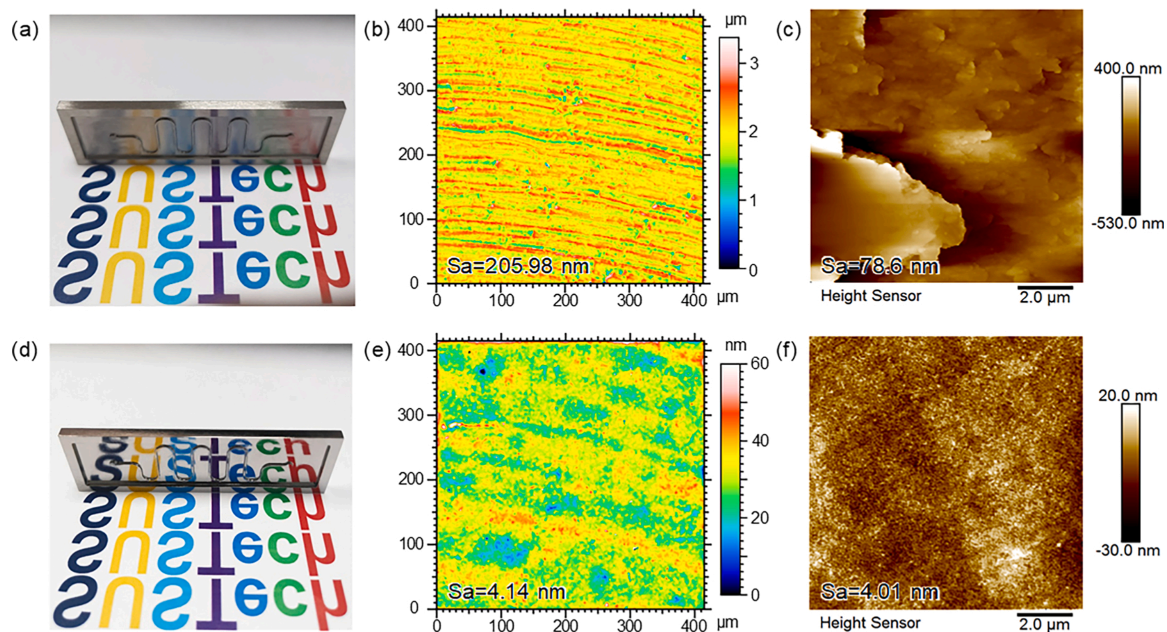

Fig. 14. Comparison of the milled mould and the mould processed by dynamic ECP. (a) Photograph of the raw mould; (b) SWLI image of the milled mould surface; (c) AFM image of the milled mould surface; (d) photograph of the polished mould; (e) SWLI image of the polished mould surface; and (f) AFM image of the polished mould surface.

Credit author statement

Xingying Zhou: Performing the experiments and data collection and analysis; Writing the manuscript.
Fang Wang: Sample preparation and measurement of the samples.
Xinquan Zhang: Supervision of the study, and evaluation of the results.
Hui Deng: Supervision of the study and revision of the manuscript.

Declaration of Competing Interest

The authors report no declarations of interest.

Acknowledgements

This work was financially supported by Shanghai Pujiang Program (19PJ1404500) and the research fund for International Cooperation (GJHZ20180928155412525) from the Science and Technology Innovation Committee of Shenzhen Municipality. The authors also would like to thank the Shenzhen High-level Innovation and Entrepreneurship Fund (No. KQTD20170810110250357) for their financial support. The authors acknowledge the assistance of SUSTech Core Research Facilities.

References

Altan, T., Lilly, B.W., Kruth, J.P., König, W., Tönshoff, H.K., Van, C.A., Khairy, A.B., 1993. Advanced techniques for die and mold manufacturing. CIRP Ann. Manuf. Technol. 42, 707–716.
Andersson, H., Van, A., 2004. Microfabrication and microfluidics for tissue engineering: state of the art and future opportunities. Lab Chip 4, 98–103.
Beck, T.R., Alkire, R.C., 1979. Occurrence of salt films during initiation and growth of corrosion pits. J. Electrochem. Soc. 126, 1662–1666.
Caire, J.P., Chainet, E., Nguyen, B., Valenti, P., 1993. Study of a new stainless-steel electropolishing process. AESF Annual Technical Conference 149–156.
Chen, L., Luo, G., Liu, K., Ma, J., Yao, B., Yan, Y., Wang, Y., 2006. Bonding of glass-based microfluidic chips at low-or room-temperature in routine laboratory. Sens. Actuators B 119, 335–344.
Dominick, W.D., Berhane, B.T., Mecomber, J.S., Limbach, P.A., 2003. Covalent immobilization of proteases and nucleases to poly (methyl methacrylate). Anal. Bioanal. Chem. 376, 349–354.
Elmore, W.C., 1939. Electrolytic polishing. J. Appl. Phys. 10, 724–727.
Guo, J., Morita, S.Y., Hara, M., Yamagata, Y., Higuchi, T., 2012. Ultra-precision finishing of micro-aspheric mold using a magnetostrictive vibrating polisher. CIRP Ann. 61, 371–374.
Han, W., Fang, F., 2019. Fundamental aspects and recent developments in electropolishing. Int. J. Mach Tool. Manuf. 139, 1–23.
Hopenfeld, J., Cole, R.R., 1966. Electrochemical machining-predicition and correlation of process variable. ASME J. Eng. Industry 755–765.
Huang, C.Y., Kuo, C.H., Hsiao, W.T., Huang, K.C., Tseng, S.F., Chou, C.P., 2012. Glass biochip fabrication by laser micromachining and glass-molding process. J. Mater. Process. Technol. 212, 633–639.
Jacquet, P.A., 1936. The mechanism of electrolytic polishing of Copper. CR Acad. Sci. 202, 402.
Lee, B.K., 2014. Microinjection molding of plastic microfluidic chips including circular microchannels. Polym. Eng. Sci. 54, 42–50.
Madou, M.J., Lee, L.J., Daunert, S., Lai, S., Shih, C.H., 2001. Design and fabrication of CD-like microfluidic platforms for diagnostics: microfluidic functions. Biomed. Microdevices 3, 245–254.
Prihandana, G.S., Mahardika, M., Nishinaka, Y., Ito, H., Kanno, Y., Miki, N., 2013. Electropolishing of microchannels and its application to dialysis system. Procedia CIRP 5, 164–168.
Saka, N., Eusner, T., Chun, J.H., 2008. Nano-scale scratching in chemical–mechanical polishing. CIRP Ann. 57, 341–344.
Strehblow, H., Ives, M.B., 1976. On the electrochemical conditions within small pits. Corros. Sci. 16, 317–321.
Suzuki, N., Haritani, M., Yang, J.B., Hino, R., Shamoto, E., 2007. Elliptical vibration cutting of tungsten alloy molds for optical glass parts. CIRP Ann. 56, 127–130.
Takagi, J., Yamada, M., Yasuda, M., Seki, M., 2005. Continuous particle separation in a microchannel having asymmetrically arranged multiple branches. Lab Chip 5, 778–784.
Tan, A., Rodgers, K., Murrihy, J.P., O'Mathuna, C., Glennon, J.D., 2001. Rapid fabrication of microfluidic devices in poly (dimethylsiloxane) by photocopying. Lab Chip 1, 7–9.
Wang, Y.Q., Yin, S.H., Huang, H., Chen, F.J., Deng, G.J., 2015. Magnetorheological polishing using a permanent magnetic yoke with straight air gap for ultra-smooth surface planarization. Precis. Eng. 40, 309–317.
Wang, F., Zhang, X., Deng, H., 2019. A comprehensive study on electrochemical polishing of tungsten. Appl. Surf. Sci. 475, 587–597.
Zhang, L., Wang, W., Ju, X.J., Xie, R., Liu, Z., Chu, L.Y., 2015. Fabrication of glass-based microfluidic devices with dry film photoresists as pattern transfer masks for wet etching. RSC Adv. 5, 5638–5646.
Zhou, T., Yan, J., Masuda, J., Oowada, T., Kuriyagawa, T., 2011. Investigation on shape transferability in ultraprecision glass molding press for microgrooves. Precis. Eng. 35, 214–220.